

# Four-terminal resistance of a ballistic quantum wire

R. de Picciotto\*, H. L. Stormer\*†, L. N. Pfeiffer\*, K. W. Baldwin\* & K. W. West\*

\* Bell-Labs, Lucent Technologies, Murray Hill, New Jersey 07974, USA

† Departments of Physics and Applied Physics, Columbia University, New York 10003, USA

The electrical resistance of a conductor is intimately related to the relaxation of the momentum of charge carriers. In a simple model, the accelerating force exerted on electrons by an applied electric field is balanced by a frictional force arising from their frequent collisions with obstacles such as impurities, grain boundaries or other deviations from a perfect crystalline order<sup>1</sup>. Thus, in the absence of any scattering, the electrical resistance should vanish altogether. Here, we observe such vanishing four-terminal resistance in a single-mode ballistic quantum wire. This result contrasts the value of the standard two-probe resistance measurements of  $h/2e^2 \approx 13 \text{ k}\Omega$ . The measurements are conducted in the highly controlled geometry afforded by epitaxial growth onto the cleaved edge of a high-quality GaAs/AlGaAs heterostructure. Two weakly invasive voltage probes are attached to the central section of a ballistic quantum wire to measure the inherent resistance of this clean one-dimensional conductor.

Electronic transport with no scattering can occur in nanoscale solid-state devices<sup>2-8</sup>. Conceptually, the simplest of these structures is the ballistic one-dimensional wire<sup>6-8</sup>, in which the transverse motion is quantized into discrete modes, and the longitudinal motion is free. In this case electrons are envisioned to propagate freely down a clean narrow pipe. However, the actual resistance of such a wire is found to be very different from zero. Instead, its value is the resistance quantum ( $R_0 = h/2e^2$ ) divided by the number of occupied transverse modes<sup>9</sup>. Hence, in the quantum limit, when the pipe is sufficiently narrow to support only a single mode, the resistance of a perfect wire is rather large:  $R_0 \approx 13 \text{ k}\Omega$ .

The origin of this resistance is best appreciated in the framework of a model for one-dimensional conduction proposed by Landauer<sup>10,11</sup>. We consider two electron reservoirs connected by a perfect single-mode wire. To maintain a current,  $I$ , through the wire, a higher electrochemical potential is imposed on the right-hand side (r.h.s.) reservoir,  $\mu_r^{\text{in}}$ , than on the left-hand side (l.h.s.) reservoir,  $\mu_l^{\text{in}}$ . Electrons that propagate through the wire to the left, away from the r.h.s. reservoir, maintain its electrochemical potential,  $\mu_l = \mu_r^{\text{in}}$ . Conversely, electrons that propagate to the right maintain the electrochemical potential of the l.h.s. reservoir,  $\mu_r = \mu_l^{\text{in}}$  (see Fig. 1c). In the absence of scattering, these electrochemical potentials do not vary along the wire.

However, although both  $\mu_l$  and  $\mu_r$  are uniform throughout the length of the wire, both vary at its ends, where the wire is connected to the reservoirs. These steps arise from electron scattering that equilibrates left movers and right movers with the local electrochemical potential of the reservoir. The variations in  $\mu_l$  and  $\mu_r$  can be viewed as contact resistances to the wire<sup>12,13</sup>, each having a value  $R_c = R_0/2$ . This is the origin of the relatively high resistance observed in two-terminal measurements on a quantum wire. On the other hand, within the wire the electrochemical potentials are independent of position and the result of a four-terminal resistance measurement should be zero, in the ideal case. We will refer to this as vanishing 'intrinsic resistance'.

Here we report the realization of a four-terminal geometry, which allows us to measure this intrinsic resistance of a quantum wire. The wires are fabricated from GaAs/AlGaAs heterostructures using the cleaved-edge overgrowth (CEO) technique<sup>14</sup> as illustrated in Fig. 1a.

The resultant wire resides all along an atomically precise edge of a GaAs quantum well. The quantum well itself supports a two-dimensional electron gas (2DEG) that is coupled to the wire from the side. We use prefabricated top gate electrodes (see Fig. 1a) to shape this 2DEG sheet. Biasing any one of the gates depletes the 2DEG underneath and creates a stretch of one-dimensional wire in front of it, which is now separated from the 2DEG. The width of the gate defines the length of this isolated wire section, and the 2DEG areas on either side conveniently serve as source and drain contacts to the wire. This geometry lends itself to a straightforward

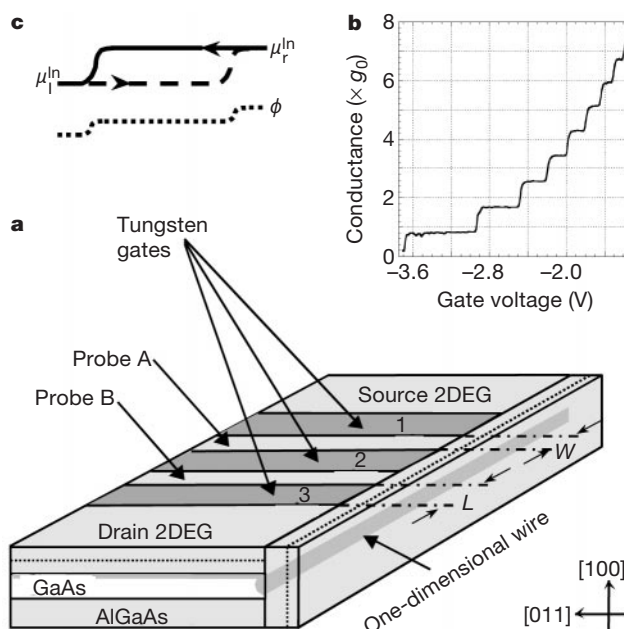


**Figure 1** Electronic transport in cleaved-edge overgrowth quantum wires. **a**, Geometry of the CEO device. The fabrication starts with a high-quality 2DEG created by epitaxial growth of a unilaterally doped GaAs quantum well onto a [001] GaAs substrate. The resultant 2DEG has a carrier density  $n_s \approx 2.5 \times 10^{11} \text{ cm}^{-2}$ , and mobility  $\mu \approx 4 \times 10^6 \text{ cm}^2 \text{ V}^{-1} \text{ s}^{-1}$ . Subsequently, this wafer is cleaved inside the MBE chamber to expose a clean and atomically smooth [110] surface, which is immediately overgrown with a modulation-doped epitaxial-layer sequence. The additional remote Si dopants that are introduced by this overgrowth step lead to a higher electron density near the cleaved edge of the quantum well. As in conventional modulation-doped samples, a strong built-in electric field binds this excess charge to the cleaved-edge interface, creating one-dimensional bound states all along the edge of the GaAs quantum well. This wire contains about 10 electronic modes and coexists with a 2DEG that resides in the quantum-well plane and couples to the wire from the side. To separate the 2DEG from the wire, prefabricated tungsten gate electrodes (for example, gate 1) are used. They deplete the 2DEG underneath them but preserve the one-dimensional channel in this region along the edge. The width of the tungsten gate defines the length,  $L$ , of the isolated wire section. Increasing the gate voltage beyond depletion of the 2DEG provides a convenient tool to control the number of occupied one-dimensional modes in this wire section. Three gates allow us to separate out four distinct 2DEG regions (see text). **b**, A representative result of a two-terminal conductance measurement of a CEO wire at a temperature,  $\theta = 300 \text{ mK}$ . For this measurement, only one electrode (say, number 1) is activated, which creates in its front a  $2\text{-}\mu\text{m}$ -long section of an isolated one-dimensional wire. Clear conductance plateaux arise, attesting to the high quality of the wire. Practically identical behaviour is observed for the wire sections in front of all electrodes (not shown). The value of the quantized resistance is somewhat larger than the universal value of  $R_0^{7,8,19}$ . The origin of this deviation is non-ideal coupling between the CEO wire and its 2DEG source and drain contacts<sup>19</sup>. Because the goal of the present paper is the determination of the intrinsic wire resistance by a four-probe measurement, which is insensitive to any contact resistance, this non-ideal current injection is inconsequential. **c**, The spatial behaviour of the electrochemical potentials of left and right movers,  $\mu_l$  and  $\mu_r$  respectively, and of the electrical potential,  $\phi$ , in a two-terminal geometry.

two-probe measurement on a quantum wire. Figure 1b shows the high-quality, quantized conductance steps that are observed in such a specimen as successive one-dimensional sub-bands are depopulated.

To create the more complex contacting geometry for a four-probe measurement, we use a pattern of three successive electrodes (numbers 1–3 in Fig. 1a). This configuration establishes two narrow 2DEG strips (A and B), that serve as voltage taps into the central portion of the wire. The wide 2DEG regions to the far right and far left serve as source and drain contacts for the current, as in the two-probe case. This gate configuration offers unique flexibility. Activating only electrode 2 provides a two-terminal measurement on the central section of the wire. Biasing all three electrodes creates an extended quantum wire along the edge and separates voltage probes A and B from the source and drain respectively. This allows us to perform a four-probe measurement on the same central section of the wire. Such a small change in the biasing scheme of our CEO sample switches directly from two-probe to four-probe geometry with marked consequences.

Figure 2 shows the result of a two-probe and a four-probe measurement on the same CEO quantum wire. The width of each

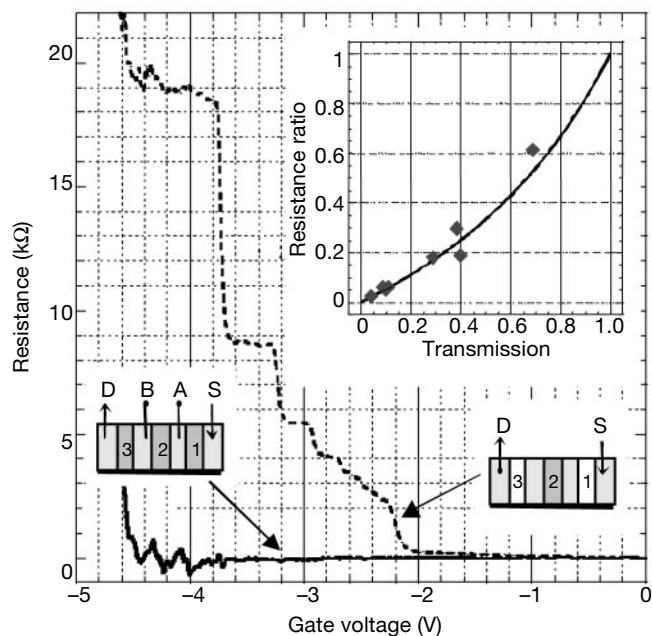


**Figure 2** Two- and four-terminal resistances of a ballistic quantum wire. The dashed line shows the two-terminal resistance of the 2- $\mu\text{m}$ -long central section of the wire versus the voltage applied to the associated gate 2. Gates 1 and 3 are not activated. The solid line shows the four-terminal resistance,  $(V_A - V_B)/I$ , versus the voltage applied to gate 2. Here  $V_A$  and  $V_B$  are the voltages at probes A and B respectively and  $I$  is the current driven from source to drain. For this measurement, the voltages applied to gates 1 and 3 correspond to a single mode in the wire sections in front of these gates. Measurements were performed at a temperature of  $\theta = 300$  mK with an excitation current smaller than 1 nA. While the two-terminal resistance moves through the characteristic quantized resistance steps, the four-terminal resistance fluctuates around zero indicating that the inherent resistance of a clean one-dimensional wire is vanishingly small. The small oscillations around zero resistance (from  $-3.8$  V to  $-4.5$  V) suggest that mesoscopic variation of the various transmission amplitudes with the one-dimensional density dominate the resistance in this regime. Indeed a similar, although not identical, pattern is observed upon successive cool-downs of the same device. As expected, similar mesoscopic variations are observed when a magnetic field is applied (see Fig. 3). Inset, probe invasiveness in a quantum wire. Diamonds, the ratio between the four-terminal and two-terminal resistances versus the invasiveness of the voltage probes (see text). Solid line, theoretical prediction of the Landauer–Buttiker model<sup>16</sup> (see text). All measurements are for single-mode wires.

gate electrode is  $L = 2 \mu\text{m}$ . The gates are separated by 2DEG strips of width  $W = 2 \mu\text{m}$  each. For the four-probe measurement electrodes 1 and 3 are set to maintain a single transverse mode in the respective wire sections, whereas these gates are not activated in the two-probe case. In both measurements the bias to the central electrode is scanned, depopulating successive one-dimensional sub-bands. As is evident from Fig. 2, the two-terminal resistance moves through the characteristic quantized resistance steps, whereas the four-terminal resistance hovers around zero resistance, with small mesoscopic fluctuations superimposed. This is the central result of our experimental work: the inherent resistance of a clean one-dimensional wire is vanishingly small.

It demonstrates experimentally that the specific two-terminal resistance value stems from an existing ‘contact resistance’ between the wire and the two macroscopic electron reservoirs at either end. In a two-terminal resistance measurement this inherent contact resistance adds to the intrinsic resistance of the wire and hence, even for a perfect wire, the two-terminal resistance is at least  $R_0$  per mode<sup>13</sup>. We will now discuss in detail the physics of two-probe versus four-probe measurements on a quantum wire.

A four-terminal geometry is a common method used to circumvent contributions from the contacts to the measured resistance. Typically, a current is driven by two contacts at the far ends of a long rectangular specimen. The electrochemical potential drop along the current path is determined by two separate voltage probes, located near the centre of the specimen, far away from the current contacts. To deduce the intrinsic resistivity, it is essential that the voltage probes do not disturb the current flow. In two or three dimensions, this is readily accomplished by using small voltage probes that leave contiguous regions of the specimen intact. In one dimension this cannot be accomplished for obvious geometrical reasons and voltage probes are always ‘invasive’. This invasiveness of a voltage probe is intimately related to the probability that an electron passing the probe will scatter into it<sup>15–19</sup>. In general, the transmission probability of left movers,  $T_l$ , and right movers,  $T_r$ , may differ.

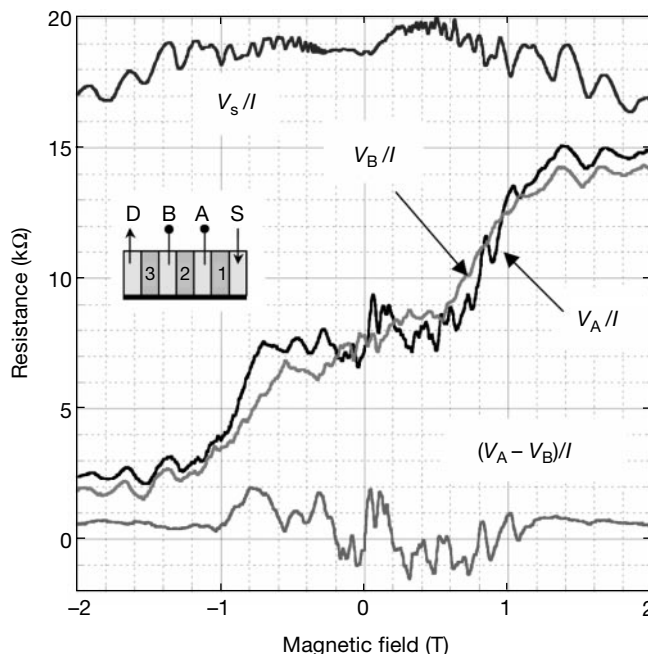


**Figure 3** Magnetic field dependence of probe coupling. Magnetic field dependence of the two-terminal ( $V_S/I$ ), three-terminal ( $V_A/I$  and  $V_B/I$ ) and four-terminal ( $(V_A - V_B)/I$ ) resistances. The sections of the wire in front of all three gates support a single mode. The invasiveness of both probes is about 4%. The voltages at both taps vary from  $V \approx V_S$  (voltage at source) at large positive field to  $V \approx V_D = 0$  (voltage at drain) at large negative field.

Yet, in the simplest case of symmetric coupling, the invasiveness is proportional to  $T = T_1 = T_r = \frac{1}{2}(R_{2r}/R)$  with  $R_{2r}$  and  $R$  being the two-terminal resistance and the resistance of the probe–wire interface respectively. The smaller  $T$  is, the less invasive is the voltage probe, leaving the wire practically undisturbed<sup>17,19</sup>.

The results shown in Fig. 2 correspond to a device with two 2- $\mu\text{m}$ -wide 2DEG probes. The resistance between each probe and wire is about 250 k $\Omega$  (not shown) indicating that their invasiveness is merely about 4%. Moreover, the overall source–drain resistance of the three wire sections in front of the electrodes, each having one occupied transverse mode, is about 20 k $\Omega$  (not shown). This value is only slightly larger than the 19  $\Omega$  two-terminal resistance of the 2- $\mu\text{m}$ -long central section (see Fig. 2), whereas classically we would have expected at least a tripling of the resistance. The absence of a significant increase of the overall resistance further indicates the low invasiveness of the voltage probes and the negligible back scattering in the wire.

Our device geometry allows extensive control over the 2DEG–wire coupling and hence over the invasiveness of a contact to a CEO wire. For example, the gap between electrodes 1 and 2 controls the invasiveness of probe A. It can be made weaker (stronger) by reducing (increasing) the width,  $W$ , as compared to the two- to one-dimensional scattering length. This scattering length was previously determined to be approximately 6  $\mu\text{m}$  in our wires<sup>19</sup>, and is easily achieved with electrode separation established by standard photolithography.

The inset of Fig. 2 shows a plot of the ratio,  $\alpha$ , of the four-terminal to the two-terminal resistance, against the transmission,  $T$ . We find that  $\alpha$  increases monotonically with  $T$ , approaching unity together with  $T$  itself. These data are in good agreement with theoretical predictions<sup>16</sup> for a four-terminal measurement with symmetrically coupled probes of invasiveness  $T$ :  $\alpha = T/(2 - T)$ . It clearly demonstrates the crucial role played by the invasiveness of the voltage probes in a four-terminal resistance measurement of a ballistic quantum wire. In the limit of fully invasive probes,  $T \rightarrow 1$ , the voltage probes essentially break the wire into three separate pieces and thus defeat their purpose, because in this limit a four-terminal measurement yields the same value as a two-terminal one. These results demonstrate the special role played by quantum coherence in the series addition of one-dimensional wires. A very invasive voltage probe acts as a strong inelastic scatterer that collapses the gap between the electrochemical potentials of left and right movers<sup>17</sup>. Such a collapse at the location of each probe leads to the well known addition rule for classical resistors.

In a ballistic one-dimensional wire, left and right propagating electrons acquire two distinct electrochemical potentials. This behaviour is unique to one dimension and is a direct result of the absence of back scattering. The idea of a local electrochemical potential, and therefore of the meaning of a voltage measurement, is thus exceptional in a ballistic wire. A voltage measurement corresponds to the value of the probe's electrochemical potential required to null the probe–sample current. In diffusive samples the probe acquires the local electrochemical potential of the neighbouring sample region. In a ballistic wire, however, the electrochemical potential required to null the probe–wire current is, in general,  $\mu_p = \alpha\mu_l + \beta\mu_r$ , with  $\alpha = T_l/(T_r + T_l)$  and  $\beta = T_r/(T_r + T_l)$ . For example, a probe that couples only to left movers ( $T_l = 1$  and  $T_r = 0$ ) will measure  $\mu_l$  while a probe that couples only to right movers will measure  $\mu_r$ . A ballistic wire has two distinct electrochemical potentials and thus there are many ways to define the internal resistance.

This ambiguity can be resolved by requiring charge neutrality. The spatial charge density of electrons, when averaged over a length scale larger than the screening length, is always compensated by a fixed positive background charge, leaving the sample as a whole neutral. In two or three dimensions, this implies  $\mu(x) - \phi(x) = C$ , with  $\phi$  the local potential and  $C$  a translation invariant constant.

Thus, the electrochemical potential difference in a four-terminal configuration yields the potential drop between voltage probes. On the other hand, in one dimension charge neutrality implies  $\mu(x) - \phi(x) = C$ , with  $\bar{\mu} = (\mu_l + \mu_r)/2$  (see Fig. 1c). Therefore, only a symmetric voltage probe, with  $T_r = T_l$  and thus  $\mu_p = \bar{\mu}$ , can measure the local one-dimensional potential. This analogy between the one-dimensional case and the two- to three-dimensional case makes it seem natural<sup>15</sup> to define the intrinsic resistance of a ballistic wire in terms of  $\bar{\mu}$ , rather than in terms of  $\mu_l$  or  $\mu_r$ .

The voltage probes of our four-terminal geometry are highly symmetric. To illustrate this, we measure the voltage of each probe,  $V_A$  and  $V_B$ , with respect to the drain. We find both voltages to be about half the voltage applied from source to drain, although the distance from the drain to probe A is twice the distance to probe B. This result shows that both probes measure  $\bar{\mu}$  regardless of their location and also confirms the view of two equal 'contact resistances' existing at each end of the wire. To further illustrate the effect of the probe–wire coupling symmetry, we measure  $V_A$  and  $V_B$  as a function of a magnetic field applied perpendicular to the quantum-well plane, as shown in Fig. 3. The effect on the 2DEG is small since at 1 T the filling factor is  $\nu \approx 10$ . With increasing positive magnetic field, the voltage at both probes increases, and saturates at approximately 1 T with a value close to the source voltage. Conversely, a negative magnetic field reduces the voltages to a value close to the voltage of the drain. This voltage swing originates from the Lorenz force exerted on the carriers. A positive (negative) magnetic field forces the left-moving (right-moving) electrons in the wire closer to the 2DEG probes. Hence the magnetic field breaks the symmetry of the coupling by establishing preferential coupling between the probes and either left or right movers, depending on the field direction. When only left (right) movers couple to the probes their voltages approach the source (drain) voltage. To fully break this symmetry requires a magnetic field of about 1 T, which corresponds to a magnetic length of approximately 250  $\text{\AA}$ , in good agreement with the width of our wire of about 200  $\text{\AA}$ .

Thus we were able to perform four-terminal resistance measurements on ballistic quantum one-dimensional wires and observed a vanishing resistance. This demonstrates experimentally that the high resistance values observed in two-probe measurements on such systems originate from the contacts alone, and that the intrinsic resistance is negligible. Our results validate the view of the quantized resistance being twice the minimal contact resistance to a single wire mode.  $\square$

Received 3 January; accepted 4 March 2001.

- Drude, P. Zur elektronentheorie der metalle 1 Teil. *Ann. Phys.* **1**, 566–613 (1900); Zur elektronentheorie der metalle 2 Teil, Galvanomagnetische und thermomagnetische effecte. *Ann. Phys.* **3**, 369–402 (1900).
- Heiblum, M. Tunneling hot electron transfer amplifiers (THETA): Amplifiers operating up to the infrared. *Solid State Electron.* **24**, 343–366 (1981).
- van Wees, B. J. et al. Quantized conductance of point contacts in a two-dimensional electron gas. *Phys. Rev. Lett.* **60**, 848–850 (1988).
- Wharam, D. A. et al. One-dimensional transport and the quantisation of the ballistic resistance. *J. Phys. C* **21**, L209–L214 (1988).
- van Houten, H. et al. Coherent electron focusing with quantum point contacts in a two-dimensional electron gas. *Phys. Rev. B* **39**, 8556–8575 (1989).
- Tarucha, S., Honda, T. & Saku, T. Reduction of quantized conductance at low temperature observed in 2 to 10  $\mu\text{m}$  long quantum wires. *Solid State Commun.* **94**, 413–418 (1995).
- Yacoby, A. et al. Nonuniversal conductance quantization in quantum wires. *Phys. Rev. Lett.* **77**, 4612–4615 (1996).
- Rother, M., Wegscheider, W., Bichler, M. & Abstreiter, G. in *Proc. of ICPS24* Vol. 2 (ed. Gershoni, D.) Th-P137 (World Scientific, Singapore, 1998).
- Imry, Y. in *Introduction to Mesoscopic Physics* (eds Craighead, H. G. et al.) 89–120 (Oxford Univ. Press, Oxford, 1997).
- Landauer, R. Spatial variations of currents and fields due to localized scatterers in metallic conduction. *IBM J. Res. Dev.* **1**, 223–231 (1957).
- Landauer, R. Electrical resistance of disordered one-dimensional lattices. *Phil. Mag.* **21**, 863–867 (1970).
- Imry, Y. in *Directions in Condensed Matter Physics* (eds Grinstein, G. & Mazenko, G.) (World Scientific, Singapore, 1986).
- Glazman, L. I., Lesovik, G. B. D., Khmel'nitskii, E. & Shekhter, R. I. Reflectionless quantum transport and fundamental ballistic-resistance steps in microscopic constrictions. *JEPT Lett.* **48**, 238–241 (1988).
- Pfeiffer, L. N. et al. Transport and optics in quantum wires fabricated by MBE overgrowth on the (110) cleaved edge. *Microelectron. J.* **28**, 817–823 (1997).

15. Engquist, H. L. & Anderson, P. W. Definition and measurement of the electrical and thermal resistances. *Phys. Rev. B* **24**, 1151–1154 (1981).
16. Buttiker, M. Four-terminal phase-coherent conductance. *Phys. Rev. Lett.* **57**, 1761–1764 (1986).
17. Buttiker, M. Role of quantum coherence in series resistors. *Phys. Rev. B* **33**, 3020–3026 (1986).
18. Buttiker, M. Symmetry of electrical conduction. *IBM J. Res. Dev.* **32**, 317–323 (1988).
19. de Picciotto, R. *et al.* 2D–1D coupling in cleaved edge overgrowth. *Phys. Rev. Lett.* **85**, 1730–1733 (2000).

**Acknowledgements**

We thank A. L. Moustakas, S. H. Simon, A. Yacoby and C. M. Varma for fruitful discussions.

Correspondence and requests for materials should be addressed to R.d.P. (e-mail: rd25@lucent.com).

.....  
**Superconductivity in the non-oxide perovskite MgCNi<sub>3</sub>**

**T. He<sup>\*</sup>, Q. Huang<sup>†</sup>, A. P. Ramirez<sup>‡</sup>, Y. Wang<sup>§</sup>, K. A. Regan<sup>\*</sup>, N. Rogado<sup>\*</sup>, M. A. Hayward<sup>\*</sup>, M. K. Haas<sup>\*</sup>, J. S. Slusky<sup>\*</sup>, K. Inumara<sup>\*</sup>, H. W. Zandbergen<sup>\*</sup>, N. P. Ong<sup>§</sup> & R. J. Cava<sup>\*</sup>**

<sup>\*</sup> Department of Chemistry and Princeton Materials Institute; <sup>§</sup> Department of Physics, Princeton University, Princeton, New Jersey, USA

<sup>†</sup> Department of Materials and Nuclear Engineering, University of Maryland, College Park, Maryland; and NIST Center for Neutron Research, Gaithersburg, Maryland, USA

<sup>‡</sup> Condensed Matter and Thermal Physics Group, Los Alamos National Laboratory, Los Alamos, New Mexico, USA

.....  
**The interplay of magnetic interactions, the dimensionality of the crystal structure and electronic correlations in producing superconductivity is one of the dominant themes in the study of the electronic properties of complex materials. Although magnetic interactions and two-dimensional structures were long thought to be detrimental to the formation of a superconducting state, they are actually common features of both the high transition-temperature ( $T_c$ ) copper oxides and low- $T_c$  material  $Sr_2RuO_4$ , where they appear to be essential contributors to the exotic electronic states of these materials<sup>1</sup>. Here we report that the perovskite-structured compound  $MgCNi_3$  is superconducting with a critical temperature of 8 K. This material is the three-dimensional analogue of the  $LnNi_2B_2C$  family of superconductors, which have critical temperatures up to 16 K (ref. 2). The itinerant electrons in both families of materials arise from the partial filling of the nickel  $d$ -states, which generally leads to ferromagnetism as is the case in metallic Ni. The high relative proportion of Ni in  $MgCNi_3$  suggests that magnetic interactions are important, and the lower  $T_c$  of this three-dimensional compound—when compared to the  $LnNi_2B_2C$  family—contrasts with conventional ideas regarding the origins of superconductivity.**

The variable stoichiometry compound  $MgC_xNi_3$  (where  $0.5 > x > 1.25$ ) has been previously reported; it was supposed to have a perovskite structure by analogy<sup>3,4</sup>. Neither its crystal structure nor its physical properties had been determined previously. In this study, samples with nominal formula  $MgC_xNi_3$  for  $x = 1.5, 1.25, 1.1, 1.0$  and  $0.9$  were prepared. The starting materials were bright Mg flakes (Aldrich Chemical), fine Ni powder (99.9% Johnson Matthey), and glassy carbon spherical powder (Alfa AESAR). The starting materials were mixed in 0.5-g batches, and pressed into pellets. The pellets were placed on Ta foil, which was, in turn, placed on an  $Al_2O_3$  boat, and fired in a quartz tube furnace under a mixed gas of 95% Ar and 5%  $H_2$ . The samples were heated for half an hour at 600 °C, followed by one hour at 900 °C. After cooling, they were

ground, pressed into pellets, and heated for an additional hour at 900 °C. Owing to the volatility of Mg encountered during the synthesis of this compound, 20% Mg in excess of the stoichiometric ratio was employed in the initial mixtures. The structural determination, described below, indicated that the compound formed was stoichiometric in metals and that no excess Mg remained in the samples.

The crystal structure of a superconducting sample ( $T_c \equiv 7.3$  K, determined magnetically) of nominal composition  $MgC_{1.25}Ni_3$  was determined by powder neutron diffraction (Fig. 1). The formula for the superconducting phase was found to be  $MgC_{0.96}Ni_3$ . The compound has the classical cubic perovskite structure, space group  $Pm\bar{3}m$ , with lattice parameter  $a = 3.81221(5)$  Å. The positions for the atoms are: Mg 1a (0,0,0); C 1b (0.5,0.5,0.5); and Ni 3c (0,0.5,0.5). The temperature factors are 0.90(3), 0.54(4), and 0.75(1) Å<sup>2</sup> for Mg, C and Ni, respectively. Refinements were performed with variable stoichiometry allowed for the C site. The C site occupancy was found to be 0.960(8), making the exact stoichiometry  $MgC_{0.96}Ni_3$ . In agreement with what is expected from the nominal composition, a small amount of unreacted graphite (2 wt%) was found in the sample. The sensitivity of the superconductivity to the C content of the perovskite phase made it necessary for carbon excess to be added to the initial mixtures to ensure attainment of the superconducting composition. The perovskite crystal structure for  $MgCNi_3$  is shown in the inset to Fig. 1. Comparison to a familiar oxide perovskite such as  $CaTiO_3$ , for example, indicates the structural equivalencies between Ca and Mg, Ti and C, and O and Ni.

The magnetic characterization of the superconducting transitions is shown in Fig. 2. The magnetic onset for the superconducting transition ranges between 7.1 K for a nominal carbon content of 1.1 per  $MgC_xNi_3$  to 7.4 K for nominal carbon content  $x = 1.5$ . The superconducting transition turns off abruptly for nominal C contents between  $x = 1.1$  and  $x = 1.0$ . All samples in the range of carbon contents shown appear to be single phase by powder X-ray diffraction (which would not be sensitive to the presence of graphite

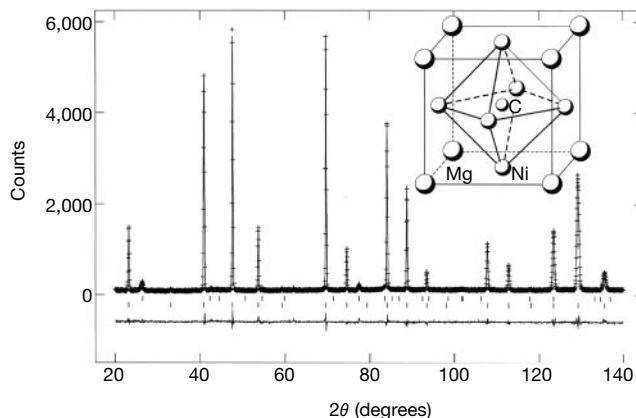


**Figure 1** The powder neutron diffraction pattern at ambient temperature for the sample of nominal composition  $MgC_{1.25}Ni_3$  and the perovskite crystal structure for the superconducting compound  $MgCNi_3$  (inset). Neutrons of wavelength 1.5402 Å were employed (Cu 311 monochromator), with collimators of 15', 20' and 7' of arc before and after the monochromator, and after the sample, respectively. The neutron scattering lengths employed in the structure refinement were 0.538, 0.665 and 1.030 (cm<sup>-1</sup>) for Mg, C and Ni, respectively. Data are shown as crosses, and the difference plot between model and data shown directly below. The vertical lines (bottom) show the Bragg peak positions for the  $MgCNi_3$  phase. The sample contains 2 wt% graphite (about 25 mol.%) in agreement with the nominal composition. Positions of the graphite peaks are shown as vertical lines above those for  $MgCNi_3$ . The refinement agreement, weighted profile agreement, and  $\chi^2$  values obtained were  $R = 5.14\%$ ,  $R_w = 6.39\%$  and  $\chi^2 = 1.258$ , indicating the high quality of the structural model.